Noncontact atomic force microscopy imaging mechanism on Ag(110): Experiment and first-principles theory

V. Caciuc,[1] H. Hölscher,[1,2,*] D. Weiner,[1,2] H. Fuchs,[1,2] and A. Schirmeisen[1,2]
[1]*Physikalisches Institut, Westfälische Wilhelms Universität Münster, Wilhelm-Klemm-Strasse 10, 48149 Münster, Germany*
[2]*Center for NanoTechnology (CeNTech), Heisenbergstrasse 11, 48149 Münster, Germany*
(Received 16 August 2007; revised manuscript received 19 November 2007; published 17 January 2008)

In this study, we analyze the noncontact atomic force microscopy (NC-AFM) imaging mechanism on the Ag(110) surface by experiment and *ab initio* theory. The experimental NC-AFM images exhibit atomic-scale resolution in the topography and dissipation signal. Interestingly, the maximum of the damping signal is between the maxima of the topography image. Comparing the geometry of the Ag(110) surface with the topography of a simulated NC-AFM image, we found that the first surface layer silver atoms are imaged as maxima in the topographic NC-AFM images. The overall structure and the corrugation height of the theoretical NC-AFM image are in good agreement with the experimental ones. Furthermore, the analysis of the short-range tip-sample interactions calculated at specific lattice sites revealed strong hysteresis effects. Our simulations also indicate that clean silicon tips might become contaminated with silver atoms during a NC-AFM experiment. Indeed, the NC-AFM experiments showed that the Ag(110) surface is difficult to image probably due to contamination of the silicon tip during the imaging process.

DOI: 10.1103/PhysRevB.77.045411 PACS number(s): 79.60.Bm, 68.37.Ps, 71.15.Dx

I. INTRODUCTION

In the past decade, noncontact atomic force microscopy (NC-AFM) emerged as an important tool in surface science due to its ability to image all kinds of surfaces with true atomic resolution in ultrahigh vacuum (UHV).[1–3] This scanning probe method is used to image the real-space topography of surfaces by sensing the interaction between an atomically sharp tip attached to a vibrating cantilever and the surface under consideration.

Another remarkable feature of NC-AFM is its ability to monitor the energy dissipation while scanning over the surfaces under study. Sometimes the corresponding dissipation images obtained simultaneously with the topographical ones also reveal atomic-scale resolution.[1,4–7] Since the atomic features of these dissipation images might be linked to the material properties of the investigated surfaces, the physical origin of the energy dissipation is the focus of current scientific discussions (see, e.g., Refs. 8–10 and references therein).

However, the mechanism of the atomic-scale contrast experimentally observed in NC-AFM images is well understood for semiconductors and insulators. The theoretical studies performed for Si(111)-(5×5),[11,12] InP(110),[13,14] GaAs(110),[15,16] and InAs(110) (Refs. 17 and 18) systems clearly showed that the atomic contrast on semiconducting surfaces is due to the short-range chemical tip-sample interaction forces involving the dangling bonds of the tip apex atom as well as the surface atoms. Similar investigations carried out for insulating surfaces[4,19–23] emphasized a similar contrast mechanism based on the short-range electrostatic interaction forces.

Although metallic surfaces were frequently imaged with atomic resolution[24–26] and sometimes used as substrates for organic molecules,[27–29] the origin of the atomic-scale contrast on the metallic surfaces is less examined. So far, only the NC-AFM contrast formation on Cu(001) surface was investigated by means of *ab initio* simulations.[30,31] In that study, it was suggested that the NC-AFM atomic contrast originates from a weak reversible short-range electrostatic interaction caused by charge transfer between an oxidized tip and the copper surface. For clean silicon tips or those contaminated with copper atoms, however, they found that the imaging mechanism resembles closely that of semiconductor surfaces, i.e., the tip-sample interactions exhibit a strong covalent character.

In this paper, we report on a combined experimental and theoretical study performed to gain insight into the nature of the NC-AFM imaging process on a Ag(110) surface. Silver surfaces have unique properties, which are exploited in many catalysis processes. However, only a few previous NC-AFM studies have reported atomic-scale images, which seem to be a general difficulty on metal surfaces. Since this might be caused by strong short-range forces in combination with atomic-scale mechanical relaxations at the tip-sample interface, a detailed understanding of those processes is necessary from the experimental and the theoretical point of view. Understanding of those atomic interaction eventually allows complex processes for the bottom up construction of atomic-scale structures on silver.[32]

In our experiments, we observed that the atomically resolved NC-AFM images exhibit an inverted contrast in simultaneously recorded topographic and energy-dissipation channels. The simulated approach and retraction force curves at specific lattice sites allowed us to interpret the maxima in the topographical NC-AFM images to originate from the first-layer silver atoms. If the AFM tip is positioned between the first-layer atomic rows, the *ab initio* calculations reveal that the interaction of reactive silicon tips with the Ag(110) surface leads to a strong hysteresis in the force curves, eventually resulting in the removal of Ag atoms from the surface. This feature leads to a tip contamination with silver atoms providing an explanation why this surface is particularly difficult to image in NC-AFM experiments.

II. EXPERIMENTAL RESULTS

The experiments were performed with a commercial ultrahigh vacuum atomic force microscope based on the beam deflection principle (VT-AFM from Omicron Nanotechnology, Germany). The measurements were done at a base pressure of 2×10^{-10} mbar at room temperature. As sensors, we used rectangular monocrystalline silicon cantilevers with a nominal tip radius of 2 nm (SSS-NCHR, Nanosensors). The spring constant $c_z=18$ N/m was calculated from the width and length of the cantilever beam and the measured resonant frequency[33] of $f_0=267.9$ kHz. The quality factor of $Q=8140$ was determined by ring-down experiments. The frequency shift signal was measured with a frequency demodulator (easy-PLL, nanoSurf AG, Switzerland). Before the experiments, the tip was shortly sputtered (4 min) with Ar ions in UHV to remove possible contaminations. The sample was a (110)-oriented Ag single crystal (Mateck GmbH, Germany), which was cleaned by repeated cycles of Ar-ion sputtering and subsequent annealing. The tip and sample were both grounded during all measurements. The experiments were carried out in a dedicated UHV surface science system placed on a vibration-free foundation.

In noncontact atomic force microscopy, the cantilever is oscillated in a self-excitation mode[34] at its fundamental eigenfrequency f_0 above the sample surface. The measured quantity in dynamic force microscopy is the frequency shift $\Delta f:=f-f_0$ with respect to the eigenfrequency f_0 of the cantilever, which depends on the tip-sample interaction. The oscillation amplitude A is kept constant by adjusting the excitation amplitude by an automatic gain control. The change of the excitation amplitude is recorded as the damping signal, which is directly related to the energy dissipation between the tip and sample.[35] Atomically resolved surface images are obtained by keeping the frequency shift Δf at a fixed value, which is correlated to a constant tip-sample interaction. Topography information is then given by regulating the movement of the cantilever base up and down. The dissipation channel is recorded simultaneously with the frequency shift during the scan process.

Figure 1 shows an image of the freshly prepared Ag(110) surface obtained with a moderate frequency shift set point of $\Delta f=-95.7$ Hz. The topography revealed large terraces of about 100 nm in diameter. Fringes can be observed at the step edges. The same effect has been previously observed in scanning tunneling microscopy (STM) experiments [see Fig. 4(d) in Ref. 36] and has been explained by the tip induced mobility of the Ag atoms at the step edges. However, in the present study, we focused on atomically flat terraces without defects or steps and scanned a small area of 2×2 nm^2 to obtain the atomically resolved topography, as shown in Fig. 2(a). For this high resolution measurement, the tip-sample distance was decreased by increasing the frequency shift to a larger negative value of $\Delta f=-265.8$ Hz. The expected rows of silver atoms in the $[1\bar{1}0]$ direction can be clearly seen, as well as the individual atoms within the rows. A comparison with the theoretical results, which will be presented in Sec. III, allows us to assign the observed maxima to the top layer silver atoms.

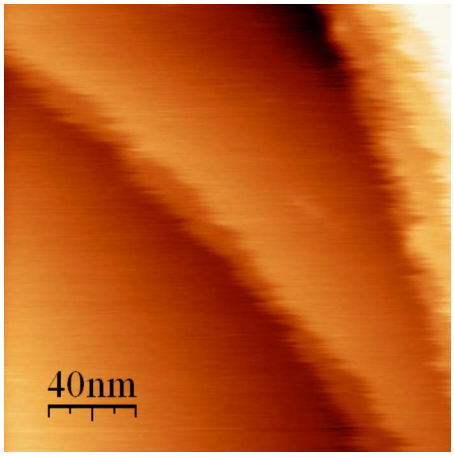

FIG. 1. (Color online) Topographic scan of Ag(110) surface with NC-AFM at a frequency shift of $\Delta f=-95.7$ Hz with a scan size of 200×200 nm^2. This image shows a terrace with a typical diameter of 100 nm. As previously reported in STM experiments (Ref. 36), fringes can be observed at the step edges.

The distance between neighboring rows is 409 pm and the distance between individual atoms within the row is 290 pm. Simultaneously with the topography, the dissipation signal was recorded, as depicted in Fig. 2(b). Here, a considerable contrast develops as well, indicating less dissipation on top of the atoms in the rows in comparison to the position between the rows. Along the $[1\bar{1}0]$ direction of the rows, no significant contrast is resolved.

For a better quantitative analysis, in Fig. 3, we show line profiles along different crystallographic directions, as indicated by the dotted arrows in Fig. 2. The topography and dissipation line profiles along the [100] direction in Fig. 3(a) show significant modulations in both signals. The height corrugation is $\Delta z=10.7\pm0.3$ pm, which is comparable to values obtained from atomic resolution images using NC-AFM on other metal surfaces.[24,26] There is also a significant modulation of the energy dissipation of $\Delta E_{diss}=94\pm7$ meV/cycle. However, the maxima of the energy dissipation coincide exactly with the minima in the topography. Thus, the energy dissipation is highest when the tip is above the atoms of the second layer, i.e., in between the rows of the top layer atoms.

The line profiles in Figs. 3(b) and 3(c) show the topography and dissipation along the $[1\bar{1}0]$ direction for two positions: above the top layer atoms (top) and above the second-layer atoms (bottom). Along the rows of the top layer atoms, the apparent height corrugation is $\Delta z=7.4\pm0.3$ pm, while the dissipation shows no systematic variation along the $[1\bar{1}0]$ direction for neither position.

It is important to note that stable imaging on the Ag surface with atomic resolution was difficult to achieve. Nevertheless, atomic resolution imaging in topography as well as in dissipation was obtained with different tips in different experimental runs. Interestingly, in those cases, we could consistently reproduce the characteristic feature that the maximum of the damping signal is located *in between* the rows of the corrugation maxima. We also measured frequency shift versus distance spectroscopy curves, which,

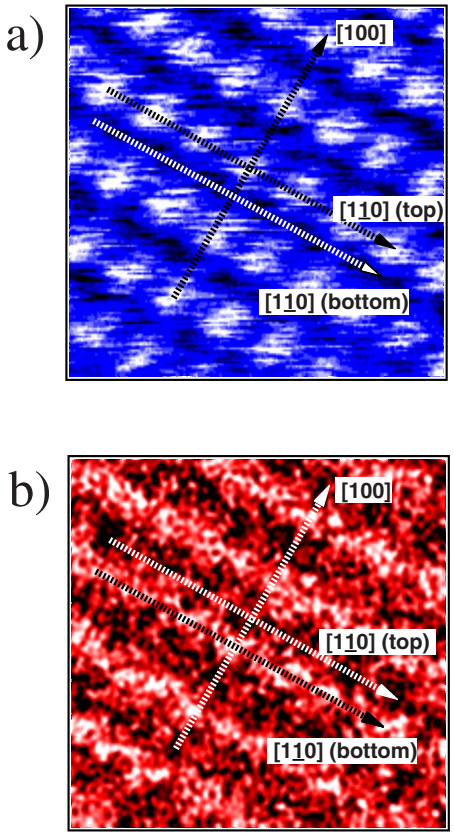

FIG. 2. (Color online) (a) Raw data of topography measured on a 2×2 nm^2 scan on Ag(110) at a frequency shift of $\Delta f=-265.8$ Hz and an amplitude of $A=9$ nm. The bright maxima are identified as the top layer atoms of the Ag(110) surface. (b) Simultaneously measured energy-dissipation signal showing a contrast opposite to the topography. Lateral drift was corrected according to the expected values for the lattice constants using the software implemented in the microscope software.

however, showed irreproducible features as soon as the tip-sample distance was below a certain value. As a consequence, stable imaging with atomic resolution on Ag(110) was only possible in a very limited regime of purely attractive tip-sample forces well before the observation of a minimum in the frequency shift versus distance curves.

III. THEORETICAL RESULTS

A. Computational method

A central difficulty in NC-AFM is the fact that the shape of the macroscopic AFM tip and, in particular, the atomic structure of the tip apex are not known. The starting point in tackling this problem is by decomposing the tip-sample interaction forces in short- and long-range contributions.[37,38] The long-range forces such as van der Waals or electrostatic forces do not lead to atomic resolution but add an offset to the frequency shift. Therefore, we decompose the AFM tip into a macroscopic part for the evaluation of the long-range forces and a nanotip, which is used to calculate to short-range tip-sample interaction forces responsible for the atomic-scale contrast in NC-AFM.

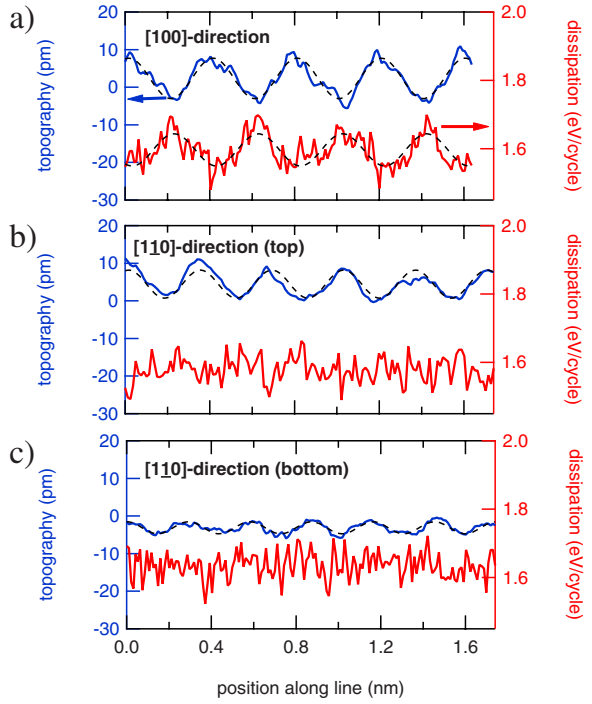

FIG. 3. (Color online) (a) Line profile along the [100] direction as indicated by the dotted line in Fig. 2 showing the simultaneously measured topography (blue) and dissipation signals (red). The topography maxima coincide exactly with the dissipation minima. [(b) and (c)] Line profiles along the [1$\bar{1}$0] (top) and [1$\bar{1}$0] (bottom) lines, respectively. The underlying dashed lines are fits to the measured line profiles used to determine the atomic corrugation along the different crystallographic directions.

The *ab initio* results reported in this study have been obtained in the framework of density functional theory[39,40] using the generalized gradient approximation[41] for the ex-

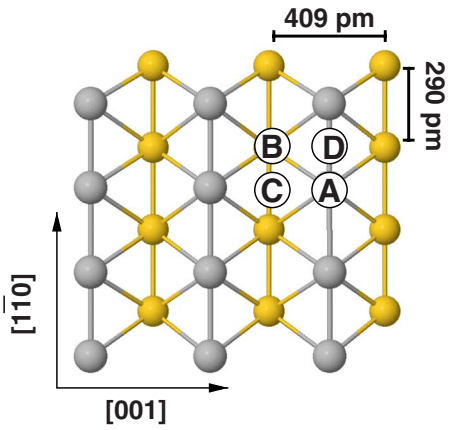

FIG. 4. (Color online) Top view of the Ag(110) surface. For clarity, the first-layer silver atoms are plotted in gray, while the second-layer atoms are displayed in yellow. The letter A indicates the position of a first-layer Ag atom (*A* site). The *B* site marks the position of a second-layer Ag atom and the *C* site corresponds to the hollow site. The saddle point between two top layer atoms is denoted as *D* site.

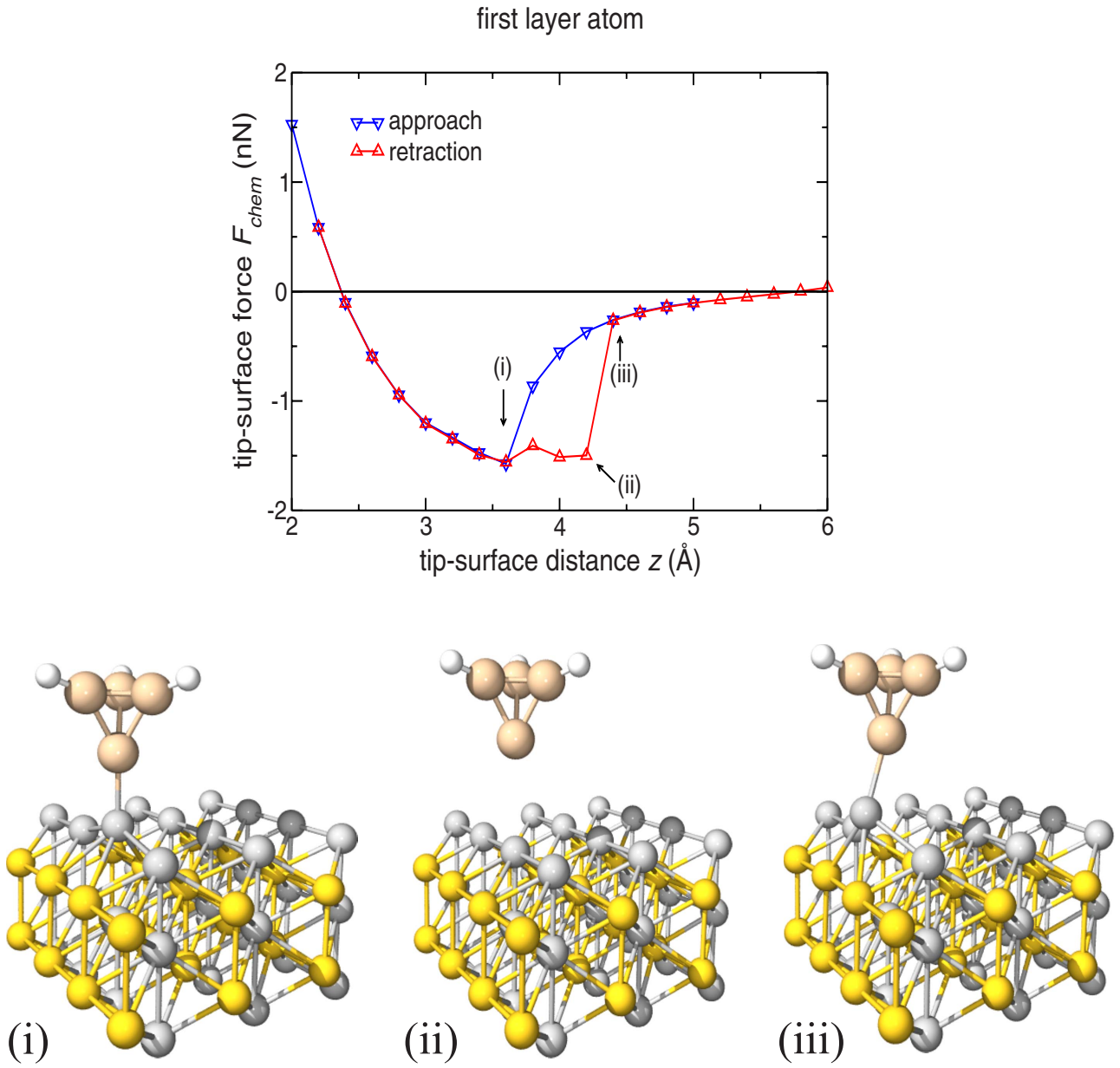

FIG. 5. (Color online) The calculated tip-sample interaction forces at a first-layer Ag atom (*A* site). Bond-formation and bond-breaking processes on the approach and retraction paths lead to an energy dissipation of about 0.5 eV. The calculated atomic structure at three distinguished tip-sample positions marked as (i), (ii), and (iii) in the force curve are shown at the bottom of the figure. The relaxed geometry depicted in (i) corresponds to a bond-formation process at a tip-sample distance of 3.6 Å when the AFM tip approaches the Ag(110) surface. A bond-breaking process takes place on the retraction path as illustrated in (ii) and (iii) for two consecutive tip-sample distances of 4.2 and 4.4 Å, respectively.

change correlations. The total energy calculations have been carried out using the pseudopotential method[42] as implemented in the ESPRESSO package.[43] The ultrasoft pseudopotentials[44] employed in our study are those provided by this package. The Kohn-Sham eigenfunctions were expanded in a plane-wave basis set determined by a cutoff energy E_{cut} of 30.0 Ry, while for the augmentation charge, we used a cutoff energy of 300.0 Ry. The Brillouin zone integrations have been done using two special k points[45] in the irreducible part of the surface Brillouin zone.

The Ag(110)-(3×4) surface was modeled by a periodic slab consisting of five atomic layers separated by a vacuum region of $\approx$15 Å. For the nanotip, we employed a Si_4H_3 cluster which represents the "sharpened" part of a silicon tip cut along the [111] direction of the bulk silicon.[46,47] The effect of the tip-sample interactions on the geometry of the Si_4H_3-Ag(110) system was investigated by relaxing the front atom of the tip and the atoms of the first two surface layers while all other atoms were kept fixed. To obtain reliable relaxed geometries of this system, the accuracy of the calculated Hellmann-Feynman force was better than 5×10^{-4} Ry/a.u. We carefully checked the presented results with respect to the k-point mesh and cutoff energies.

B. Tip-sample interaction at specific lattice sites

The basic focus of our *ab initio* simulations is to understand the microscopic origin of the experimentally observed NC-AFM contrast inversion in the topographic images with respect to the dissipation images recorded on the Ag(110) surface. For this purpose, we calculated the short-range tip-sample interaction forces at four distinct lattice sites marked in Fig. 4. The Si_4H_3 nanotip was placed on top of a Ag atom of the first (*A* site) and the second surface layer (*B* site). In addition, an approach and retraction of the tip above the middle point between two Ag atoms from two adjacent atomic $[1\bar{1}0]$ rows were simulated (hereafter denoted as the hollow site or *C* site) as well as an approach curve on top of the saddle point denoted as *D* site.

The resulting force versus distance curves when the tip approaches and retracts from the Ag(110) surface are shown in Figs. 5–7 for the *A*, *B*, and *C* sites, respectively. The tip-sample distance z in the theoretical force curve plots is the vertical distance between the Si apex atom of the AFM tip and the first-layer Ag surface atoms in their equilibrium ground state structure.[13,16] Animated ball-and-stick models of the approach and retraction of the tip on the three different sites are available as auxiliary material[56]

A peculiar feature of the calculated approach and retraction force curves is the occurrence of a substantial hysteresis when the tip is above a first-layer silver atom (*A* site, Fig. 5) and a hollow site (*C* site, Fig. 7). Interestingly, there is almost no hysteresis for the tip on top of the second-layer Ag atom. This effect might be attributed to the symmetry at this point and hysteresis might occur if the tip is approached and retracted at a slightly different lateral position. However, the hysteresis for the tip on top of the first-layer Ag atom is moderate, leading to an energy dissipation of ≈0.5 eV, but it is much larger when the tip is oscillated above the hollow site (see Fig. 7) due to the adsorption of a Ag atom by the tip.

By comparing the three different curves, one can also easily observe that the deepest minimum is obtained for the AFM tip on top of the second-layer Ag atom (see Fig. 6). Here, the largest attractive force is larger than 2 nN. Initially, one is tempted to conclude that a silver atom from the *second* surface layer should thus be imaged as a protrusion. However, this strong tip-sample interaction occurs only at very small tip-surface distances of 2.0–2.5 Å, which are not reached during stable imaging. The maximal attractive force of the first-layer Ag atom, though, occurs at larger distances of about 3.5–4 Å.

Besides the topography, we also measured the energy dissipation in the experiments. However, before drawing a direct comparison with the obtained dissipation images, it is necessary to discuss the different mechanical responses of the surface atoms at the different sites. The analysis of the relaxed geometries of the tip-surface system shows that when the tip is above the first-layer Ag atom, the system behaves stably until a jump occurs at ≈3.6 Å. Only then does the observed hysteresis develop, which is related to bond-formation and bond-breaking processes with the top Ag atom. Stable NC-AFM imaging on the atomic scale as in Fig. 2(a), however, implies that the tip-sample distances will be larger than the position of this force minimum, since a stable

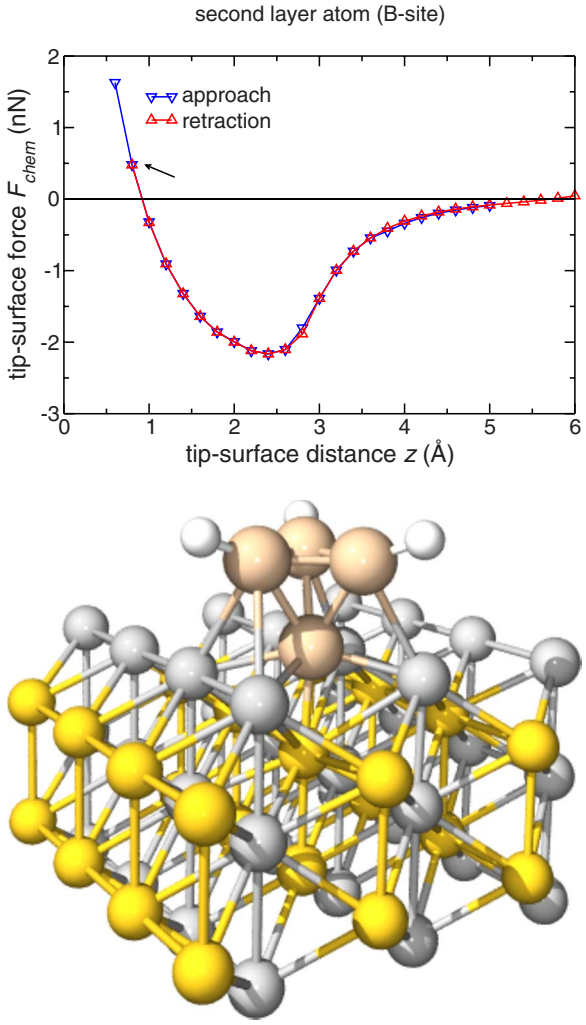

FIG. 6. (Color online) The calculated tip-sample interaction forces at a second-layer Ag atom (*B* site). There is almost no hysteresis between the approach and retraction paths. The ball-and-stick model on the right shows the atomic structure of the tip-sample geometry the position marked by an arrow in the force curve. This relaxed configuration obtained in the repulsive regime shows the formation of multibonds between the tip and surface. In particular, this presence of multiple bonds is a fingerprint of AFM operating in the repulsive part of the tip-sample interaction forces.

feedback system requires continuously decreasing negative frequency shifts, which can be roughly related to the regime of increasing attractive forces before the force minimum.[48,49] In addition to this condition, we have to consider that the mechanical instabilities caused by the hysteresis might prevent stable imaging conditions. Therefore, we do not expect to reach the regime of the strong atomic hysteresis during imaging of the top layer atom rows and conclude that atomic resolution is only possible for distances larger than 3.6 Å.

The interaction of the AFM tip with second-layer Ag atom rows shows strong atomic relaxation effects on the hollow-site position, as depicted in Fig. 7, eventually even leading to the removal of a single Ag atom from the surface. Our *ab*

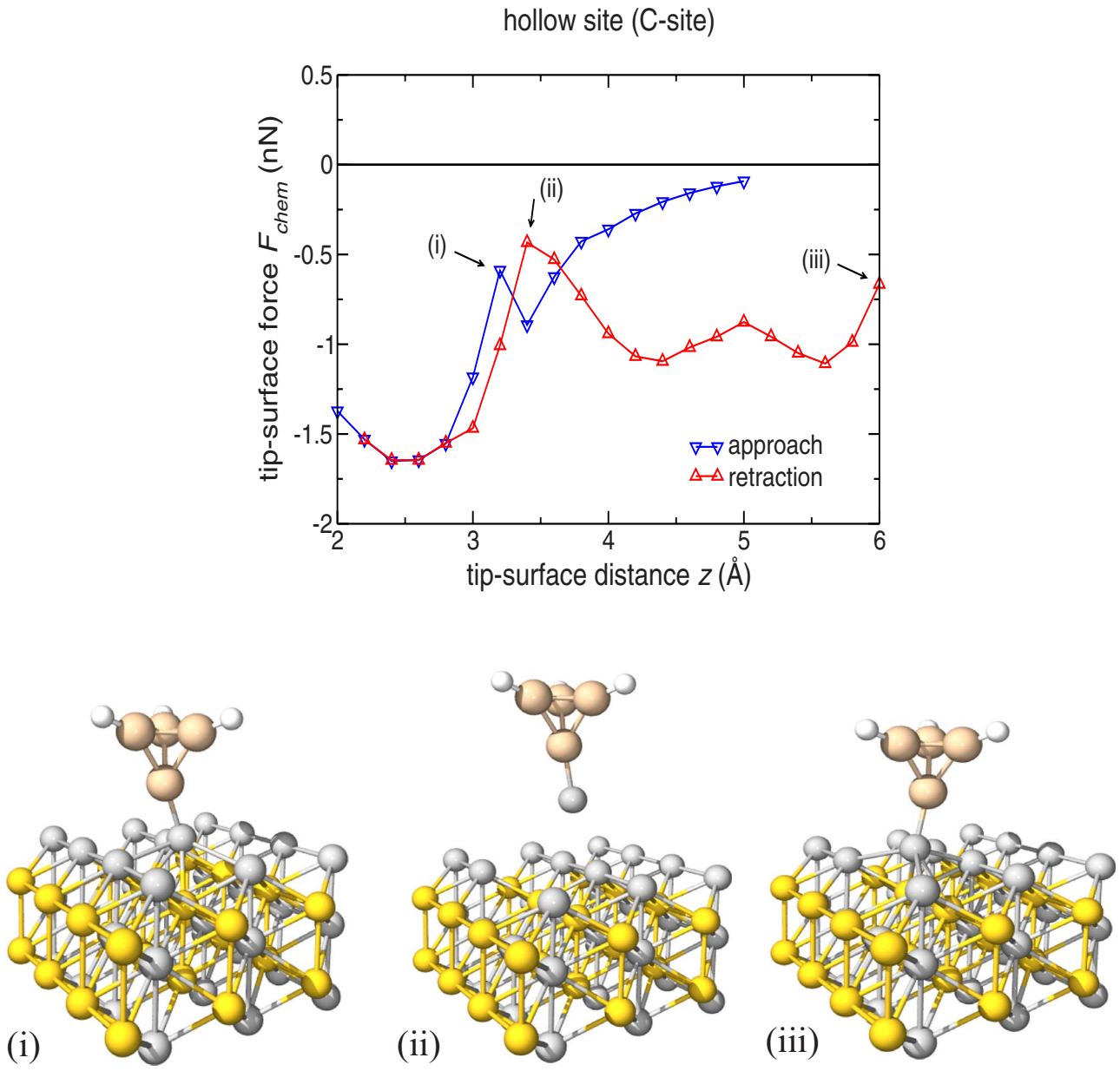

FIG. 7. (Color online) The calculated tip-sample interaction forces at a hollow site (*C* site). In this case, the AFM tip extracts a Ag atom from the surface, and thus becomes contaminated with silver. Three atomic structures at the tip-sample positions marked as (i), (ii), and (iii) in the force curve are shown at the bottom of the figure. On the approach path, at a tip-sample separation distance of 3.2 Å, a chemical bond between the silicon tip and a surface Ag atom is formed, as illustrated by the tip-surface geometry (i). When the tip moves away from the Ag(110) surface, the silicon tip interacts quite strongly with the surface on the whole retraction path. The geometry (ii) shows such a situation for a tip-sample distance of 3.4 Å. As displayed by the tip-surface relaxed geometry (iii), at a final distance of 6 Å, the silver atom is completely detached from the surface, as demonstrated by the charge density analysis displayed in Fig. 8.

initio simulations show the occurrence of complex multiple-bond-formation processes with up to five Ag surface atoms, which lead to those mechanical instabilities. Interestingly, these processes are already initiated in the regime of increasing attractive forces, significantly before the force minimum is reached, and therefore well within the regime of stable NC-AFM imaging. Nonetheless, the onset of those strong multiprocesses is a strong indication toward increased energy dissipation on the second-layer rows. This would be in agreement with the observed contrast reversal in the topography and dissipation images.

On the other second-layer site *B* (depicted in Fig. 6), we find that the substrate relaxation is fully reversible during approach and retraction. Correspondingly, we find vanishing hysteresis in the calculated force curves. However, also in this case, strong multiple bonding processes take place in the regime before the force minimum, and probably only due to the high symmetry of the chosen point, no significant hysteresis in the force curves is observed.

Turning back to the *C* site, where the tip is on top of the hollow site (see Fig. 7), our *ab initio* simulations suggest that its interaction with the surface is strong enough to even pick

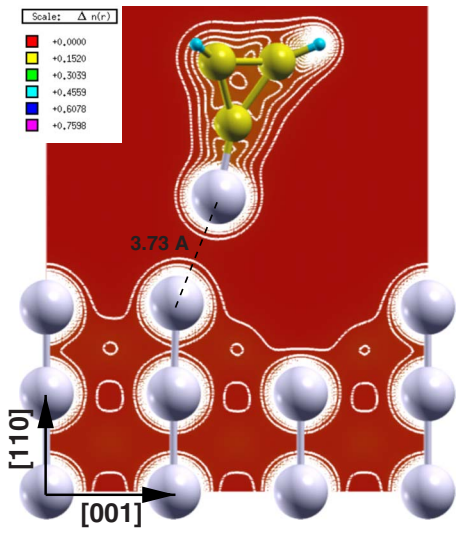

FIG. 8. (Color online) Charge density map in a plane cut along the [001] direction of the Si_4H_3-Ag(110) system. The initially clean silicon tip picked up a silver atom from the surface on the retraction path above the hollow site [see Fig. 7(i)]. The absence of the charge density between the Ag atom attached to the silicon tip and the surface clearly marks a bond-breaking process. The charge density plots have been done using the XCRYSDEN program (Ref. 55).

up an individual Ag atom from the substrate while retracting the tip. After this approach, a stable chemical bond between the silicon tip and the Ag is formed. More specifically, when the Si_4H_3 nanotip is 6.0 Å away from the surface, the distance between the Ag atom attached to the silicon tip and the closest surface atom is 3.73 Å. Assuming a covalent radius of 1.444 Å for silver atoms, calculated as the half-distance between two neighboring silver atoms in the bulk,[57] the magnitude of this separation distance suggests that a bond-breaking process took place at this lattice site during the retraction movement of the tip. This conclusion is further supported by the charge density distribution of the tip-sample system. As revealed by the charge density map in Fig. 8, the lack of charge density between the Ag atom of the tip and the surface is a clear evidence that, indeed, an initially clean silicon tip removed a silver atom from the surface.

C. Simulation of noncontact atomic force microscopy images

Since a direct comparison of the calculated short-range F_{sr} force curves with the experimental images is not possible, we simulated a complete NC-AFM image in order to compare its contrast with the experimental topography image presented in Fig. 2(a). An essential element of a simulation is to include the long-range van der Waals forces F_{vdW} acting between the macroscopic tip and the sample surface. Since these long-range forces are independent of the surface site, we model the macroscopic part of the tip by a sphere with radius $R=10$ nm. For this tip geometry, the van der Waals forces can be evaluated from $F_{vdW}(z)=-A_H R/6z^2$ where A_H is the Hamaker constant.[58] Then, the total tip-sample interaction force $F_{ts}=F_{sr}+F_{vdW}$ is used to calculate the physical

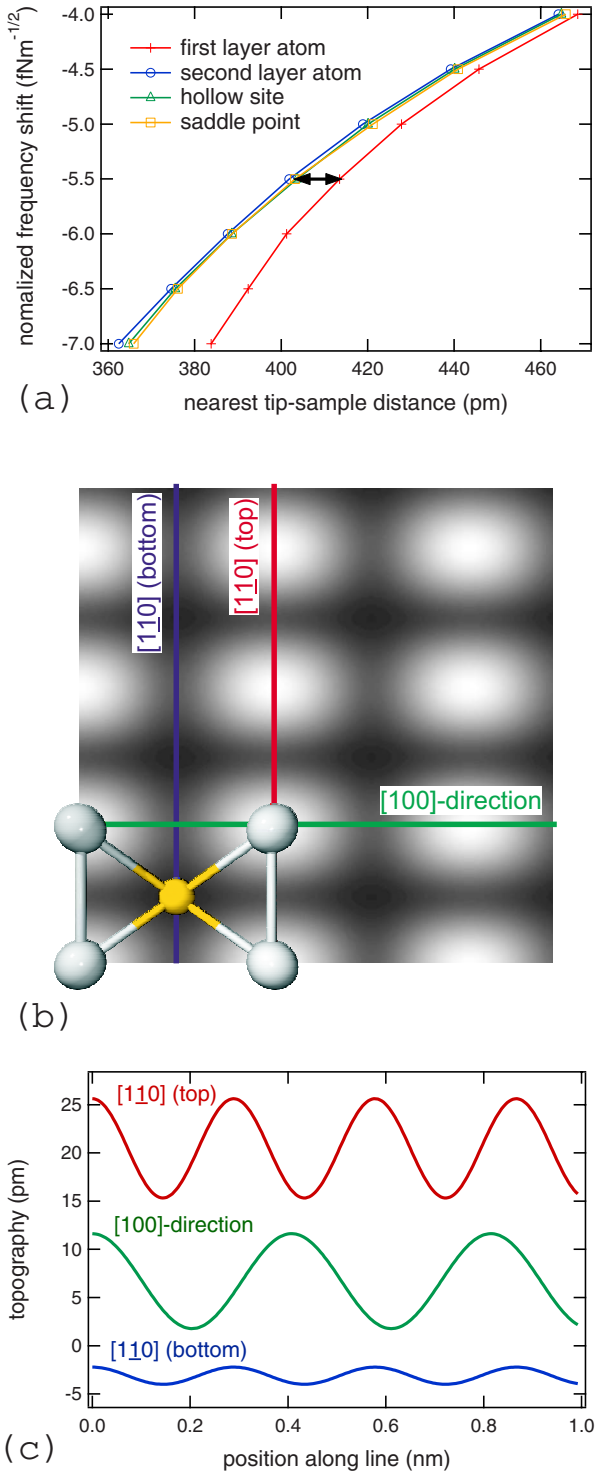

FIG. 9. (Color online) (a) The normalized frequency shift at different lattice sites. For the calculations of these curves, we considered also the long-range van der Waals forces. The black arrow marks the corrugation for a normalized frequency shift of $\gamma=-5.5$ fN m$^{1/2}$. (b) A simulated NC-AFM image for this value of the normalized frequency shift (1×1 nm^2). A comparison with the surface structure of Ag(110) allows the identification of the maxima as the first-layer Ag atoms. (c) The scan lines calculated for the positions marked in (b). A comparison with the experimental scan lines shown in Fig. 3 reveals reasonable agreement between theory and experiment.

quantity measured in a NC-AFM experiment, namely, the frequency shift,[50]

$$\Delta f(D) = \frac{1}{\sqrt{2}\pi}\frac{f_0}{c_z A^{3/2}}\int_D^\infty \frac{F_{\mathrm{ts}}(z)}{\sqrt{z-D}}dz, \quad (1)$$

where D represents the tip-surface distance of closest approach, and f_0, c_z, and A stand for the mechanical eigenfrequency, spring constant, and oscillation amplitude of the cantilever, respectively. In our analysis, we will employ the normalized frequency shift $\gamma = c_z A^{3/2}\Delta f/f_0$, which has the advantage of being independent of the actual experimental parameters A, c_z, and f_0.[51,52] The resulting normalized frequency shift curves are plotted in Fig. 9(a).

In order to simulate a map of constant frequency shift (i.e., a NC-AFM image) from these curves, we used the method proposed by Sasaki *et al.*[53] which relies on a two-dimensional Fourier expansion of the tip-sample interaction forces. Taking into account the symmetry of the substrate and keeping only the first terms in the Fourier expansion, the tip-surface forces can be written at any surface point (x,y) as

$$F_{ts}(x,y) = b_0 + b_1\cos(2\pi/a_x x) + b_2\cos(2\pi/a_y y) + b_3\cos(2\pi/a_x x)\cos(2\pi/a_y y), \quad (2)$$

where $a_x = 409$ pm and $a_y = 290$ pm are the lattice constants along the $[1\bar{1}0]$ and $[001]$ directions, respectively. All four expansion coefficients could be calculated from the four approach curves.

Finally, in order to model the behavior of the z feedback in the experimental setup, we choose a suitable normalized frequency shift γ_{const} and determine the corresponding nearest distance D at the four distinct lattice sites, i.e., we solve numerically the equation $\gamma(D) = \gamma_{const}$.[17,18]

The simulated NC-AFM image is presented in Fig. 9(b). It is important to note that this image was obtained at a tip-surface separation distance large enough to avoid the mechanical instabilities which might be induced by hysteresis in the force curves, as discussed in the previous section. By comparing the theoretical NC-AFM image with the structure of the Ag(110) surface, one can observe that only the first-layer Ag atoms are imaged as maxima. As a consequence, this outcome of our first-principles simulations allows us to unambiguously interpret the topography of the experimental NC-AFM images obtained for Ag(110) surface. Besides this, as depicted in Fig. 9(c), we analyzed the corrugation height for several scan directions. Considering the experimental uncertainties, the corrugation value shows a surprisingly good agreement with those recorded experimentally (see Fig. 3). The theoretical corrugation is 10.3 pm (experimental = 10.8 pm) along the $[1\bar{1}0]$ direction (top) and 9.8 pm (experimental = 7.4 pm) along the $[100]$ direction. The bottom line along the $[1\bar{1}0]$ direction shows a corrugation of only 1.8 pm (experimental = 3.2 pm).

IV. SUMMARY

In the presented study, we compared an experimental and a theoretical investigation of the NC-AFM imaging mechanism of silicon tips on the Ag(110) surface. In the experiments, the topographical NC-AFM images revealed an inverted contrast with respect to the simultaneously recorded dissipation images. Our first-principles calculations show that the observed maxima in the topography can be identified with the first-layer Ag atoms. This conclusion is further supported by the analysis of the topography of a simulated NC-AFM image where the corrugation height calculated for several scan directions agrees with that obtained in experiment. The calculated force curves at specific lattice sites also point to site-dependent energy-dissipation processes. The largest attractive tip-sample force occurs when the tip is on top of a second-layer Ag atom. Furthermore, when the tip is placed over a hollow site, the AFM tip pulls out an individual Ag atom from the surface. This interpretation is supported by the analysis of the charge density distribution of the system. As a consequence, the silicon tip becomes contaminated with silver atoms, which provides an explanation for the experimental difficulties for imaging the Ag(110) surface with atomic resolution.

ACKNOWLEDGMENTS

We thank Stefan Heinze (University of Hamburg) for useful discussions. The computations were performed with the help of the ZIVCLUSTER at the University of Münster. This work was financially supported in part by the DFG (Grants No. HO 2237/2-1 and HO 2237/3-1) and the BMBF (Grant No. 03N8704).

*hendrik.hoelscher@uni-muenster.de

[1] S. Morita, R. Wiesendanger, and E. Meyer, *Noncontact Atomic Force Microscopy* (Springer, Berlin, 2002).

[2] R. García and R. Pérez, Surf. Sci. Rep. **47**, 197 (2002).

[3] H. Hölscher and A. Schirmeisen, in *Advances in Imaging and Electron Physics*, edited by P. W. Hawkes (Academic, London, 2005), pp. 41–101.

[4] R. Bennewitz, A. S. Foster, L. N. Kantorovich, M. Bammerlin, C. Loppacher, S. Schär, M. Guggisberg, E. Meyer, and A. L. Shluger, Phys. Rev. B **62**, 2074 (2000).

[5] M. Guggisberg, M. Bammerlin, A. Baratoff, R. Lüthi, C. Loppacher, F. Battiston, J. Lü, R. Bennewitz, E. Meyer, and H.-J. Güntherodt, Surf. Sci. **461**, 255 (2000).

[6] R. Hoffmann, M. A. Lantz, H. J. Hug, P. J. A. van Schendel, P. Kappenberger, S. Martin, A. Baratoff, and H.-J. Güntherodt, Phys. Rev. B **67**, 085402 (2003).

[7] A. Schirmeisen, D. Weiner, and H. Fuchs, Phys. Rev. Lett. **97**, 136101 (2006).

[8] H. Hoelscher, B. Gotsmann, W. Allers, U. D. Schwarz, H. Fuchs, and R. Wiesendanger, Phys. Rev. Lett. **88**, 019601 (2001).

[9] L. N. Kantorovich and T. Trevethan, Phys. Rev. Lett. **93**, 236102 (2004).
[10] A. Schirmeisen and H. Hölscher, Phys. Rev. B **72**, 045431 (2005).
[11] R. Pérez, M. C. Payne, I. Štich, and K. Terakura, Phys. Rev. Lett. **78**, 678 (1997).
[12] R. Pérez, I. Štich, M. C. Payne, and K. Terakura, Phys. Rev. B **58**, 10835 (1998).
[13] J. Tóbik, I. Štich, R. Pérez, and K. Terakura, Phys. Rev. B **60**, 11639 (1999).
[14] J. Tóbik, I. Štich, and K. Terakura, Phys. Rev. B **63**, 245324 (2001).
[15] S. H. Ke, T. Uda, R. Pérez, I. Štich, and K. Terakura, Phys. Rev. B **60**, 11631 (1999).
[16] S. H. Ke, T. Uda, I. Štich, and K. Terakura, Phys. Rev. B **63**, 245323 (2001).
[17] V. Caciuc, H. Hölscher, S. Blügel, and H. Fuchs, Nanotechnology **16**, S59 (2005).
[18] V. Caciuc, H. Hölscher, and S. Blügel, Phys. Rev. B **72**, 035423 (2005).
[19] A. L. Shluger, L. N. Kantorovich, A. I. Liversushits, and M. J. Gillan, Phys. Rev. B **56**, 15332 (1997).
[20] A. I. Liversushits, A. L. Shluger, A. L. Rohl, and A. S. Foster, Phys. Rev. B **59**, 2436 (1999).
[21] A. S. Foster, C. Barth, A. L. Shluger, R. M. Nieminen, and M. Reichling, Phys. Rev. B **66**, 235417 (2002).
[22] A. S. Foster, O. H. Pakarinen, J. M. Airaksinen, J. D. Gale, and R. M. Nieminen, Phys. Rev. B **68**, 195410 (2003).
[23] A. S. Foster, A. Y. Gal, J. M. Airaksinen, O. H. Pakarinen, Y. J. Lee, J. D. Gale, A. L. Shluger, and R. M. Nieminen, Phys. Rev. B **68**, 195420 (2003).
[24] S. Orisaka, T. Minobe, T. Uchihashi, Y. Sugawara, and S. Morita, Appl. Surf. Sci. **140**, 243 (1999).
[25] C. Loppacher, M. Bammerlin, M. Guggisberg, F. Battiston, R. Bennewitz, S. Rast, A. Baratoff, E. Meyer, and H.-J. Güntherodt, Appl. Surf. Sci. **140**, 287 (1999).
[26] C. Loppacher, M. Bammerlin, M. Guggisberg, S. Schär, R. Bennewitz, A. Baratoff, E. Meyer, and H.-J. Güntherodt, Phys. Rev. B **62**, 16944 (2000).
[27] C. Loppacher, M. Guggisberg, O. Pfeiffer, E. Meyer, M. Bammerlin, R. Lüthi, R. Schlittler, J. K. Gimzewski, H. Tang, and C. Joachim, Phys. Rev. Lett. **90**, 066107 (2003).
[28] S. Tanaka, H. Suzuki, T. Kamikado, and S. Mashiko, Nanotechnology **15**, S87 (2004).
[29] B. Such, D. Weiner, A. Schirmeisen, and H. Fuchs, Appl. Phys. Lett. **89**, 093104 (2006).
[30] P. Dieška, I. Štich, and R. Pérez, Phys. Rev. Lett. **91**, 216401 (2003).
[31] P. Dieška, I. Štich, and R. Pérez, Nanotechnology **15**, S55 (2004).
[32] S.-W. Hla, K.-F. Braun, and K.-H. Rieder, Phys. Rev. B **67**, 201402(R) (2003).
[33] J. E. Sader, I. Larson, P. Mulvaney, and L. R. White, Rev. Sci. Instrum. **66**, 3789 (1995).
[34] T. R. Albrecht, P. Grütter, D. Horne, and D. Rugar, J. Appl. Phys. **69**, 668 (1991).
[35] H. Hölscher, B. Gotsmann, W. Allers, U. D. Schwarz, H. Fuchs, and R. Wiesendanger, Phys. Rev. B **64**, 075402 (2001).
[36] J. J. Schulz, R. Koch, and K. H. Rieder, Phys. Rev. Lett. **84**, 4597 (2000).
[37] M. Guggisberg, M. Bammerlin, C. Loppacher, O. Pfeiffer, A. Abdurixit, V. Barwich, R. Bennewitz, E. Meyer, and H.-J. Güntherodt, Phys. Rev. B **61**, 11151 (2000).
[38] S. M. Langkat, H. Hölscher, A. Schwarz, and R. Wiesendanger, Surf. Sci. **527**, 12 (2003).
[39] P. Hohenberg and W. Kohn, Phys. Rev. **136**, B864 (1964).
[40] W. Kohn and L. J. Sham, Phys. Rev. **140**, A1133 (1965).
[41] J. P. Perdew, K. Burke, and M. Ernzerhof, Phys. Rev. Lett. **77**, 3865 (1996).
[42] M. C. Payne, M. P. Teter, D. C. Allan, T. A. Arias, and J. D. Joannopoulos, Rev. Mod. Phys. **64**, 1045 (1992).
[43] S. Baroni *et al.*, http://www.pwscf.org/
[44] D. Vanderbilt, Phys. Rev. B **41**, 7892 (1990).
[45] H. J. Monkhorst and J. D. Pack, Phys. Rev. B **13**, 5188 (1976).
[46] V. Caciuc, H. Hölscher, S. Blügel, and H. Fuchs, Phys. Rev. Lett. **96**, 016101 (2006).
[47] V. Caciuc, H. Hölscher, S. Blügel, and H. Fuchs, Phys. Rev. B **74**, 165318 (2006).
[48] H. Ueyama, Y. Sugawara, and S. Morita, Appl. Phys. A: Mater. Sci. Process. **66**, S295 (1998).
[49] U. D. Schwarz, H. Hölscher, and R. Wiesendanger, Phys. Rev. B **62**, 13089 (2000).
[50] U. Dürig, Appl. Phys. Lett. **75**, 433 (1999).
[51] F. J. Giessibl, Phys. Rev. B **56**, 16010 (1997).
[52] H. Hölscher, A. Schwarz, W. Allers, U. D. Schwarz, and R. Wiesendanger, Phys. Rev. B **61**, 12678 (2000).
[53] N. Sasaki, H. Aizawa, and M. Tsukada, Appl. Surf. Sci. **157**, 367 (2000).
[54] A. Bayler, A. Schier, G. A. Bowmaker, and H. Schmidbaur, J. Am. Chem. Soc. **118**, 7006 (1996).
[55] A. Kokalj, J. Mol. Graphics Modell. **17**, 176 (1999).
[56] See EPAPS Document No. E-PRBMDO-77-015804 for the animated ball-and-stick models. For more information on EPAPS, see http://www.aip.org/pubserversus/epaps.html.
[57] Note that this value depends on the coordination of the silver atoms in a specific compound. For instance, in a two-coordinate compound, the covalent radius of Ag was found to be 1.33 Å (Ref. 54).
[58] Since we are not aware of a better value, for the system under study, we used a typical value of A_H=0.1 aJ for the presented results. However, the overall result does not change as long as the values for R and A_H are in reasonable range.